Time-resolved magneto-optical Kerr effect in the altermagnet candidate MnTe

Isaiah Gray,[1,2] Qinwen Deng,[1] Qi Tian,[1] Michael Chilcote,[3] Matthew Brahlek,[3] and Liang Wu[1]

[1)] *Department of Physics and Astronomy, University of Pennsylvania, Philadelphia, PA 19104, USA*

[2)] *Current address: Research and Exploratory Development Department, Johns Hopkins University Applied Physics Laboratory, Laurel, MD 20723*

[3)] *Materials Science and Technology Division, Oak Ridge National Laboratory, Oak Ridge, TN 37831, USA*

(*Electronic mail: liangwu@sas.upenn.edu)

(*Electronic mail: Isaiah.Gray@jhuapl.edu)

(Dated: 9 April 2024)

α-MnTe is an antiferromagnetic semiconductor with above room temperature T_N = 310 K, which is promising for spintronic applications. Recently, it was predicted to be an *altermagnet*, containing bands with momentum-dependent spin splitting; time-resolved experimental probes of magnetism in MnTe are therefore important both for understanding the magnetic structure and potential device applications. We investigate ultrafast spin dynamics in epitaxial MnTe(001)/InP(111) thin films using the time-resolved magneto-optical Kerr effect. At room temperature, we observe an oscillation mode at 55 GHz that does not appear at zero magnetic field. Combining field, polarization, and temperature dependence, we identify this mode as an acoustic phonon-coupled magnon, likely originating from inverse stimulated Raman scattering. Additionally, we observe two optical phonons at 3.6 THz and 4.2 THz, which broaden and redshift with increasing temperature.

In the past several years, antiferromagnets have been developed into active elements of spintronic devices, forming memory elements[1,2], terahertz nano-oscillators[3,4], and low-dissipation interconnects in hybrid quantum systems[5]. A natural route towards integrating these devices with traditional semiconductor functionality is to employ magnetic semiconductors[6]; while ferromagnetic semiconductors that are ordered at room temperature are rare, antiferromagnetic semiconductors are more common and offer new methods of controlling the spin degree of freedom, such as coupling between magnons and excitons[7]. An example material is hexagonal α-MnTe, promising due to its high Néel temperature $T_N \approx 310$ K[8], stable magnetoresistance reflecting Néel orientation[9], and spin-phonon coupling[10,11]. Very recently, MnTe has received increased attention after the prediction that it is not simply an antiferromagnet, but an *altermagnet*[12,13]. In this new magnetic phase, the spin-up and spin-down bands are neither degenerate, like conventional antiferromagnets, nor uniformly split, like ferromagnets; rather, the bands contain anisotropic spin polarization that alternates sign in momentum space while preserving zero net spin polarization.

This anisotropic spin polarization has very recently been observed in MnTe[14], $MnTe_2$[15], and RuO_2[16], and is predicted to lead to new effects of both scientific and practical importance, such as an anomalous Hall effect[12], an associated magneto-optical Kerr effect, and chiral magnons that can carry spin current[17]. Currently there are few experimental demonstrations of these effects, mostly in RuO_2[16,18–21]. In MnTe, there is one report of an anomalous Hall effect[22], and a magneto-optical Kerr effect has been predicted[23] but not yet observed. Experimental studies of magnetism in MnTe are therefore important, both for better understanding of a potential altermagnetic phase and more broadly as an antiferromagnetic semiconductor for spintronics.

In this letter, we perform time-resolved magneto-optical Kerr effect (TR-MOKE) measurements on hexagonal MnTe thin films as a function of temperature, polarization, and magnetic field. We identify optical phonon modes at 3.6 THz and 4.2 THz and show that they broaden and redshift with increasing temperature from 10 K to 350 K. In the presence of magnetic field, we observe an oscillation at 55 GHz which we hypothesize is due to an acoustic phonon-coupled magnon. This oscillation can be enhanced or suppressed by changing the pump polarization angle, which indicates a non-thermal origin. Oscillation components at 55 GHz persist even above the nominal $T_N = 310$ K, up to the maximum measured $T = 335$ K, which indicates that acoustic phonons as well as the magnon contribute to the TR-MOKE signal.

The structure of hexagonal α-MnTe, with space group $P6_3/mmc$, is shown in Fig. 1(a). It is an A-type antiferromagnet, containing ferromagnetic planes of in-plane Mn spins that alternate spin

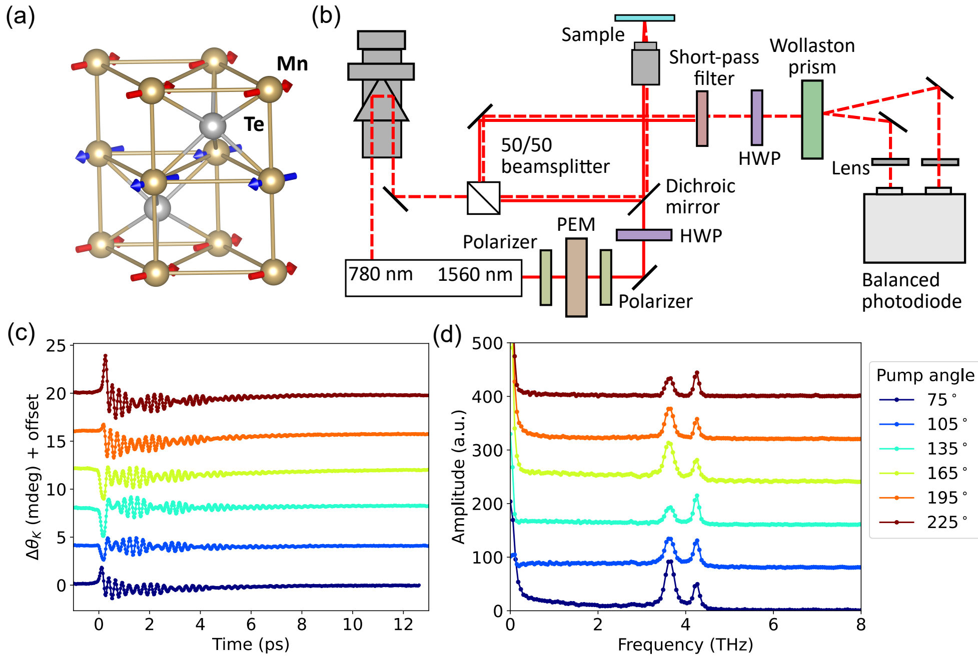

FIG. 1. Time-resolved magneto-optical Kerr effect (TR-MOKE) setup and observation of optical phonons in MnTe. (a) Crystal and magnetic structure of hexagonal MnTe (001). Gold and silver balls represent Mn and Te, respectively. (b) Schematic of two-color pump-probe MOKE with 1560 nm pump and 780 nm probe, both ∼100 fs in duration. (c) TR-MOKE scans of MnTe(001) at 295 K as a function of linear pump polarization, and (d) associated fast Fourier transforms (FFTs).

direction along the *c*-axis. The easy axis is at 30° to the crystalline *a*-axis. Our samples are 40 nm-thick MnTe(001) thin films, grown on InP(111) via molecular beam epitaxy.

We perform two-color pump-probe TR-MOKE, schematically illustrated in Fig. 1(b). We use a 1560 nm pump at 10 mW power and a 780 nm probe at 0.7 mW power on the sample; both pump and probe pulses are ≈100 fs in duration and have 80 MHz repetition rate. Both beams are focused through a 10x microscope objective at normal incidence, forming a 30 μm spot size. The reflected light is short-pass filtered to reject the pump, then the polarization rotation $\Delta\theta_K(t)$ is measured with a Wollaston prism and a balanced photodiode. The signal-to-noise is enhanced by modulating the pump between orthogonal polarization states with a PEM at 42 kHz (placed before the half-wave plate that controls pump polarization) and measuring the second harmonic of the photodiode voltage output using a lock-in amplifier. Both pump and probe are linearly polarized.

We first show short time scans (up to 13 ps) at room temperature (295 K) as a function of pump polarization angle in Fig. 1(c). After an initial sharp peak, we observe beating between two modes. Upon taking the FFTs in Fig. 1(d), we find peaks at 3.6 and 4.2 THz. These frequencies match modes observed in previous Raman spectroscopy of MnTe[10], where they were attributed to transverse and longitudinal optical phonons, respectively. We find that varying the pump polarization changes the relative amplitude of each mode. Fitting the oscillations to two damped sines, we find that at least one mode shows three-fold symmetry (shown in the supporting information), which one might expect from the hexagonal lattice. Polarization-dependent amplitudes demonstrate a non-thermal excitation mechanism, such as impulsive stimulated Raman scattering (ISRS)[24] or displacive excitation of coherent phonons (DECP)[25]. Since DECP requires absorption of a photon (meaning above-bandgap excitation), ISRS does not, and our pump wavelength is below the bandgap of MnTe(1.15 eV = 1078 nm at 295 K[26]), ISRS is the most likely excitation mechanism. Our results differ from previous time-resolved reflectivity and MOKE on MnTe[11,27], where only the doubly degenerate E_{2g} phonon mode at 5.3 THz (also seen in Raman scattering[10]) was observed. In these works, however, the pump wavelength was 800 nm (above the bandgap), the probe wavelength was 730 nm, and the pump-probe signal was explicitly attributed to DECP. These different excitation mechanisms and probe wavelengths might cause the observed differences in phonon spectra.

To look for spin oscillations, we fix the pump polarization and measure $\Delta\theta_K(t)$ at different values of applied magnetic field H_{app}. Since polar MOKE measures the out-of-plane magnetization component and the easy axis in MnTe is in-plane, we apply out-of-plane H_{app} by placing a permanent magnet behind the sample. In Fig. 2(a), we show $\Delta\theta_K(t)$ scans at 225° pump angle from horizontal, where both optical phonon modes have roughly equal amplitude, with associated FFTs in Fig. 2(b). After the initial fast phonon oscillations, we observe slower oscillations whose amplitude depends on H_{app}, and do not appear when $H_{app} = 0$. Oscillations of similar frequencies (tens of GHz) were observed in time-resolved transmissivity at 800 nm pump wavelength in MnTe/SrF_2(111) in Ref. 28, where they were tentatively attributed to acoustic phonons[29].

We fit the data from 10 ps onwards, discarding the initial phonon modes, to the sum of an exponential decay representing electron-phonon relaxation[11], two or three damped oscillations (depending on the pump angle, see the supporting information) that represent acoustic phonons and/or magnons[30], and a linear background:

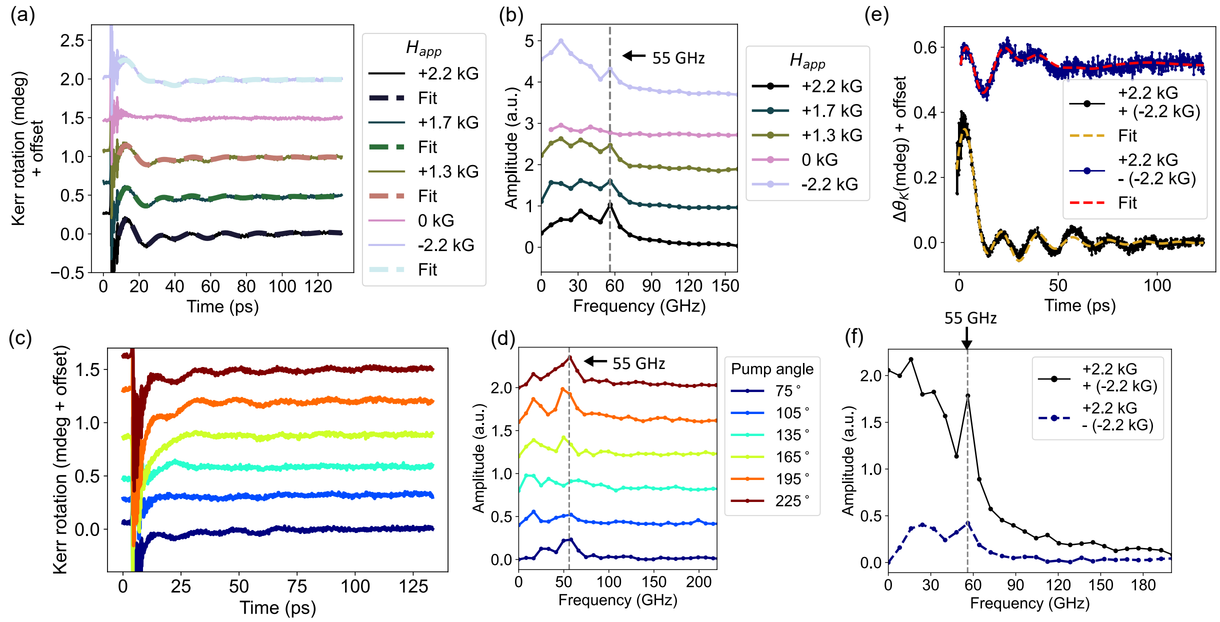

FIG. 2. Magnon and acoustic phonon oscillations at 295 K. (a) Longer scans (133 ps duration) at fixed 225° pump angle as a function of out-of-plane magnetic field H_{app}, and (b) associated FFTs. We observe a mode at 55 GHz with field-dependent amplitude, which indicates spin oscillations, as well as other features in the FFT at ∼17 GHz and 34 GHz that may represent acoustic phonons. (c) Pump polarization dependence of $\Delta\theta_K(t)$ at fixed $H_{app} = 2$ kG, with FFTs in (d). The oscillations are suppressed or enhanced as a function of pump angle, demonstrating a non-thermal origin such as phonon-induced magnons. (e) Difference and sum of $\Delta\theta_K(t)$ at +2.2 kG and -2.2 kG, and (f) associated FFTs. Both plots contain oscillation components at 55 GHz, which means non-magnetic signal cannot be straightforwardly subtracted out by subtracting opposite fields.

$$\begin{aligned}\Delta\theta_K(t) = A_{exp}e^{-t/t_0} + A_1 e^{-\alpha_1 t}\sin(2\pi f_1 t + \phi_1) \\ + A_2 e^{-\alpha_2 t}\sin(2\pi f_2 t + \phi_2) \\ + A_3 e^{-\alpha_3 t}\sin(2\pi f_3 t + \phi_3) + Bt + C\end{aligned} \tag{1}$$

Fits are shown with the data in Fig. 2(a), except at H_{app} = 0 kG, where a consistent fit could not be obtained. At this pump angle (225°), the features of the data are largely captured by two damped oscillations and using three did not significantly improve the fit quality (see the supporting information). The linear background varies from run to run and is attributed to experimental artifacts, for example from inevitable slight defocusing of the probe beam when scanning the delay line. Best fit parameters are shown in Table I. We find that although both oscillations go to zero when $H_{app} = 0$, A_1 monotonically depends on the magnitude of H_{app}, which suggests a magnetic origin, whereas A_2 does not.

Previous studies of magnons in MnTe are scarce; there is one neutron scattering report of a zone boundary magnon at 5.6 THz at 295 K[8], while A DFT study[31] calculates ≈ 0.5 THz at $k = 0$. We can estimate the $k = 0$ magnon frequencies from the anisotropy, which in MnTe is largely easy-plane. Within the easy plane there are nominally three equivalent easy axes; however, MnTe on InP(111) experiences biaxial tensile strain due to the difference in thermal coefficient between InP and MnTe[32]. This strain modifies the in-plane anisotropy in a not-well-understood manner that depends also on sample thickness. Regardless, since the in-plane anisotropy field H_{Az} is small compared to the hard-axis (easy-plane) field H_{Ax}, we can use the formula for the two $k = 0$ easy-plane magnon frequencies ω_α and ω_β[33]:

$$\begin{aligned} \omega^2_{\alpha,\beta} = \gamma^2 \{ & H_E(H_{Ax} + 2H_{Az}) + H_0^2 \\ & \pm \left[4H_0^2 H_E(H_{Ax} + 2H_{Az}) + H_E^2 H_{Ax}^2\right]^{1/2} \}, \end{aligned} \tag{2}$$

where $\gamma = g\mu_B/\hbar$ is the gyromagnetic ratio, H_E is the exchange field, and H_{Ax} and H_{Az} are the hard-axis and easy-axis anisotropy fields, respectively. For $H_{Ax} >> H_{Az}$, Eqn. 2 reduces to:

$$\omega^2_{\alpha 0} \approx \gamma^2 (2H_E H_{Ax} + 3H^2_{app}), \omega^2_{\beta 0} \approx \gamma^2 (2H_E H_{Az} - H^2_{app}), \tag{3}$$

while for $H_{app} = 0$, regardless of the anisotropy values, the frequencies are

$$\omega^2_{\alpha 0} = \gamma^2 2H_E \left(H_{Az} + H_{Ax}\right), \omega^2_{\beta 0} = \gamma^2 2H_E H_{Az}. \tag{4}$$

Although the values of H_{Az} and H_{Ax} are not well-known, we can get an estimate by using the spin-flop field $H_{SF} \approx \sqrt{2H_E H_{Az}}$, which was measured to be 2 T for MnTe/InP(111)[32]. Assuming $g = 2$ for MnTe, the in-plane magnon frequency $\omega_{\beta 0}$ evaluates to 56 GHz, consistent with our measured value. From the lack of any measurable magnetization response in MnTe with OOP field up to 6 T in Ref. 9, we can estimate that $H_{Ax} > 6$ T, which means that the out-of-plane magnon frequency $\omega_{\alpha 0} > 176$ GHz - therefore, features between 17 and 35 GHz are unlikely to be magnons. They may represent acoustic phonons, or a non-monotonic magneto-optical response to sample heating[34]. In previous studies of the easy-plane antiferromagnet NiO, the in-plane mode was observed with a linearly polarized probe through Faraday rotation, while the out-of-plane mode was observed with a circularly polarized probe through the Cotton-Mouton effect (linear birefringence)[35]. If similar mechanisms are active in MnTe, the higher-frequency magnon may only appear when using a circularly polarized probe, which will be the subject of future work.

Following the field dependence, we measure pump polarization dependence of the spin oscillations at fixed H_{app} = 2.2 kG in Fig. 2(c), with associated FFTs in 2(d). We find that the oscillation amplitudes are pump polarization-dependent - strongest at 195° and 225°, and nearly disappearing at 105° and 135° (although at the current signal-to-noise level, we cannot definitively assign them three-fold symmetry). We also note that data at some angles, such as 75°, fit better to three oscillations, while data at other angles, such as 195° and 225°, only seem to contain two. This suggests that multiple acoustic phonons with different pump angle dependences may be excited by the laser.

Pump polarization dependence of the GHz oscillations establishes a non-thermal origin, as with the optical phonons. In general, magnons measured with TR-MOKE can be thermally or non-thermally generated. In thermal generation, heating from the pump laser temporarily changes the anisotropy field H_A, which reorients the effective field H_{eff} and causes the spins to precess around the new H_{eff}[36]. Non-thermal magnon generation is often caused by spin-phonon coupling in magnetic semiconductors and insulators when the laser coherently excites phonons[37], and were observed in MnTe in Refs. 11 and 27. In those experiments, the laser excited the 5.3 THz E_{2g} optical phonon, causing the Te atoms to oscillate out-of-phase. This modulated the Mn-Te-Mn bond angle, in turn causing an oscillation in the weak Te-mediated superexchange J_3 which generated magnons at the same frequency. In our data, however, the 3.6 THz and 4.2 THz oscillations in $\Delta\theta_K(t)$ show no field dependence within experimental resolution (see the supplemental information). Therefore, we attribute them entirely to optical phonons. The polarization dependence in Fig. 2(c) is consistent with a hypothesis of acoustic phonon-induced spin oscillations at 55 GHz, driven by ISRS[24].

In some spin-phonon coupled systems, $\Delta\theta_K(t)$ contains contributions at $H_{app} = 0$ from the phonons themselves (as in Fig. 1) or from phonon-induced spin tilting[38,39]. Typically, magnetic and non-magnetic signals are separated by taking the sum and difference of data acquired at opposite magnetic fields[40]. In Fig. 2(e), we plot the sum and difference of $\Delta\theta_K(t)$ at $H_{app} = +2.2$ kG and -2.2 kG, with FFTs in 2(f). We find oscillation components at 55 GHz in both quantities, which is consistent with a non-magnetic acoustic phonon and a coupled magnon at the same frequency that both contribute to the $\Delta\theta_K(t)$ signal. Therefore, isolating magnetic from non-magnetic

TABLE I. Fit parameters for the data in Fig. 2(a), fit to Eqn. 1. Uncertainties on the last significant digit are given in parentheses.

H_{app}	2.2 kG	1.7 kG	1.3 kG	-2.2 kG
A_1 (mdeg)	0.108(5)	0.063(5)	0.039(4)	0.049(3)
α_1 (ps^{-1})	0.023(1)	0.023(2)	0.016(2)	0.026(2)
f_1 (GHz)	53.9(2)	53.3(3)	53.4(3)	56.0(5)
ϕ_1 (deg)	13(3)	12(5)	5.0(1)	-16(4)
A_2 (mdeg)	0.236(8)	0.22(1)	0.32(1)	0.345(5)
α_2 (ps^{-1})	0.084(3)	0.078(4)	0.107(4)	0.073(2)
f_2 (GHz)	36.7(5)	36.2(7)	32.8(6)	18.2(3)
ϕ_2 (deg)	14(2)	16(3)	20(2)	52(2)

contributions to $\Delta\theta_K(t)$ cannot be straightforwardly done by taking the difference and sum at low fields. Instead, we measure above T_N ($\approx$ 300 K in our thin films[41], slightly lowered from bulk T_N = 310 K due to strain), where we expect spin oscillations to disappear in a paramagnetic phase. In Fig. 3, we measure $\Delta\theta_K(t)$ time traces from 295 K to 335 K. We show scans at fixed H_{app} = +2.2 kG from 290 335 K in 3(a), and FFTs in 3(b). Surprisingly, oscillation components at 55 GHz persist at least up to 335 K, the highest temperature measured. At this temperature, the oscillations are non-magnetic; yet, a clear field dependence was seen at room temperature in Fig. 2. Our hypothesis is that $\Delta\theta_K(t)$ is due to a phonon-coupled magnon below T_N, and purely the acoustic phonon - at the same frequency - above T_N. Increased contribution of non-magnetic phonons to $\Delta\theta_K(t)$ at 335 K compared to 295 K could be caused by several factors, such as changes in the phonon density of states or the birefringence coefficient at elevated temperature. Future work will investigate these oscillations further with high-temperature magnetic field dependence.

Lastly, we measure $\Delta\theta_K(t)$ as a function of temperature from 10 K up to 350 K in a cryostat. In this configuration, the maximum attainable H_{app} was $\approx$ 500 G, which we found was not sufficient to resolve spin oscillations. Instead, we focus on the optical phonon oscillations, showing $\Delta\theta_K(t)$ traces in Fig. 4(a) and FFTs in 4(b). (Full time traces showing no spin oscillations are shown in the Supporting Information.)

To analyze the temperature dependence of the phonons, we fit the background, then subtract it off and fit the residual oscillations to two damped sinusoids. We find that this two-step process

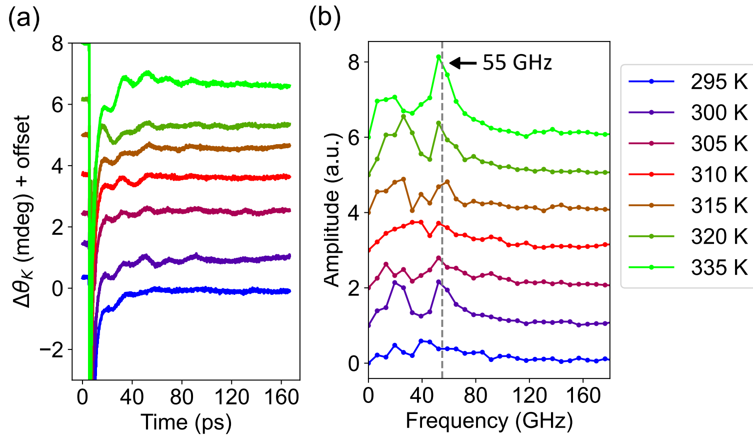

FIG. 3. Coupled spin-phonon oscillations above room temperature. (a) $\Delta\theta_K(t)$ at fixed H_{app} = +2.2 kG as a function of temperature, and (b) corresponding FFTs. Oscillations persist even above the nominal T_N = 305-310 K, indicating phonon contributions to $\Delta\theta_K(t)$ above T_N.

is more robust than fitting the background and oscillations simultaneously. At low temperatures, modeling the background by a sum of decaying exponentials does not yield a satisfactory fit. Therefore, we adapt a phenomenological model developed to to fit pump-probe reflectivity in Ref. 42:

$$\begin{aligned}\Delta T_{el}(t) &= \Delta T_{e,max}\mathrm{erf}\left(\frac{t}{\tau_{ee}}\right)e^{-t/\tau_{el}},\\ \Delta T_l(t) &= \Delta T_{l,max}\mathrm{erf}(t/\tau_0)\left(1-e^{-\frac{t+\tau_0}{\tau_{el}}}\right),\\ \Delta R/R(t) &= A\Delta T_e(t)+B\Delta T_l(t),\end{aligned} \tag{5}$$

Eqn. 5 approximates a two-temperature model in which $\Delta T_{el}(t)$ is the electron temperature, $\Delta T_l(t)$ is the lattice temperature, τ_{ee} is the electron-electron equilibration time, τ_{el} is the electron-phonon relaxation time, $\tau_0 \sim 100$ fs is the pump pulse width, and A and B are fitting amplitudes relating temperature changes to optical response. Since $\Delta\theta_K(t)$ is not identical to reflectivity, we fit to:

$$\begin{aligned}\Delta\theta_K(t) &= \Delta\theta_{K,1}(t)+\Delta\theta_{K,2}(t)\\ &= C_1\mathrm{erf}\left(\frac{t}{\tau_1}\right)e^{-t/\tau_2}+C_2\mathrm{erf}(\tau/\tau_0)\left(1-e^{-\frac{\tau+\tau_0}{\tau_2}}\right)\end{aligned} \tag{6}$$

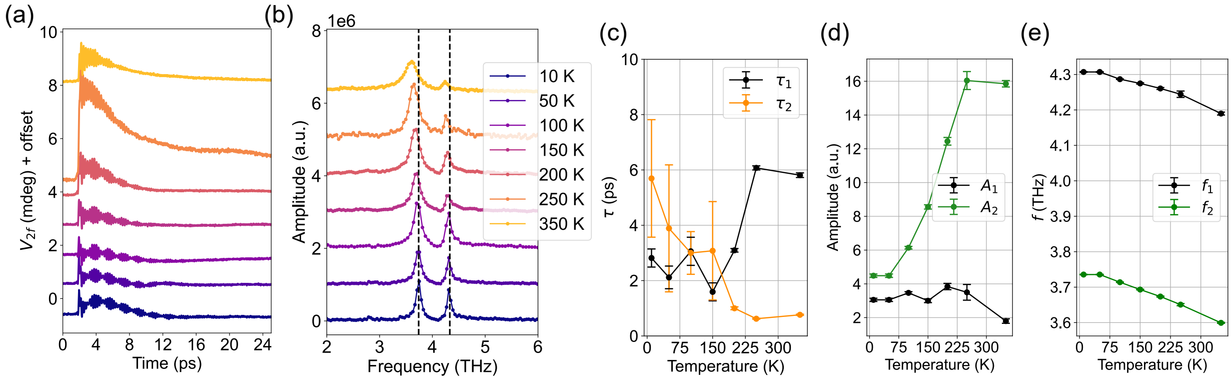

FIG. 4. Temperature dependence of the 3.6 THz and 4.2 THz optical phonons. (a) $\Delta\theta_K(t)$ traces from 10 K to 350 K and (b) corresponding FFTs. At higher temperatures, the phonons broaden in linewidth, redshift, and have shortened lifetime, in agreement with previous Raman studies. (c) Fit time scales τ_1 and τ_2 after fitting the background to a two-temperature model described in Eqn. 4. (d) Amplitudes and (e) frequencies of the two phonons, obtained by fitting to two damped sinusoids after background subtraction.

without explicitly identifying τ_1 and τ_2 with τ_{ee} and τ_{el}. Fitting results from the electron and lattice time scales are shown in Fig. 4(c). τ_1 increases with increasing T, while τ_2 decreases. Although the background is well-fit by this model (see the supplemental information for details), τ_1 is too long to be straightforwardly associated with τ_{ee}, which is typically < 1 ps. However, τ_2 is on the same order as typical τ_{el}, and the increase of τ_2 with T may correspond to the known increase of τ_{el} with increasing electron temperature[43]. Unlike Ref. 11, we do not observe a sublattice demagnetization time scale that changes dramatically above T_N, which suggests that the 3.6 and 4.2 THz phonons are unrelated to the tens of GHz spin oscillations.

After fitting the background, we fit the residual optical phonon oscillations to two damped sinusoids as in Eqn. 1: $\Delta\theta_K(t) = A_1 e^{-\alpha_1 t}\sin(2\pi f_1 t + \phi_1) + A_2 e^{-\alpha_2 t}\sin(2\pi f_2 t + \phi_2)$. The phonon fit amplitudes A_1,A_2 and frequencies f_1, f_2 are shown in Fig. 4(d) and (e). The frequencies monotonically decrease with increasing T, in agreement with previous Raman studies[10]. We find that the amplitude of the 4.2 THz phonon A_1 decreases slightly with increasing T, while A_2 (the 3.6 THz phonon) increases until it remains constant above 250 K.

In conclusion, we used TR-MOKE to identify an acoustic phonon-coupled magnon mode and two optical phonon modes in the antiferromagnetic semiconductor MnTe. Both the magnon and the optical phonon can be suppressed or enhanced by changing pump polarization, demonstrating a non-thermal origin. Somewhat surprisingly, we observe oscillations above T_N = 310 K, at least up to 335 K, which reflects temperature-dependent contributions of both phonons and magnons to $\Delta\theta_K(t)$ and will be the subject of future work. Our results provide new insight into this unique magnetic system, and will be important as MnTe continues to be studied for spintronic and altermagnetic applications.

ACKNOWLEDGMENTS

I.G. was mainly sponsored by the Army Research Office under the grant No. W911NF-20-2-0166. The construction of the pump-probe setup was supported by the Air Force Office of Scientific Research under award no. FA9550-22-1-0410. Q.D. was supported by the NSF EPM program under grant no. DMR-2213891 and the Vagelos Institute of Energy Science and Technology graduate fellowship. This work was also supported by the U. S. Department of Energy (DOE), Office of Science, Basic Energy Sciences (BES), Materials Sciences and Engineering Division (growth and materials characterization).

DATA AVAILABILITY STATEMENT

The data that support the findings of this study are available from the corresponding author upon reasonable request.

AUTHOR DECLARATIONS

Conflict of Interest

The authors have no conflicts to disclose.

AUTHOR CONTRIBUTIONS

Isaiah Gray: Conceptualization (equal); Data curation (lead); Formal analysis (lead); Methodology (equal); Validation (lead); Software (supporting); Visualization (lead); Writing - original draft (lead); Writing - review and editing (equal). **Qinwen Deng**: Data curation (supporting); Formal analysis (supporting); Methodology (equal); Software (equal). **Qi Tian:** Methodology (equal); Software (equal). Michael Chilcote: Resources (equal). **Matthew Brahlek:** Resources (equal); Writing - review and editing (equal). **Liang Wu:** Conceptualization (equal); Funding Acquisition (lead); Methodology (equal); Project Administration (lead), Supervision (lead), Writing - review and editing (equal).

REFERENCES

[1] P. Wadley, B. Howells, J. Železný, C. Andrews, V. Hills, R. P. Campion, V. Novák, K. Olejník, F. Maccherozzi, S. S. Dhesi, S. Y. Martin, T. Wagner, J. Wunderlich, F. Freimuth, Y. Mokrousov, J. Kuneš, J. S. Chauhan, M. J. Grzybowski, A. W. Rushforth, K. W. Edmonds, B. L. Gallagher, and T. Jungwirth, "Electrical switching of an antiferromagnet," Science **351**, 587–590 (2016).

[2] T. Higo, K. Kondou, T. Nomoto, M. Shiga, S. Sakamoto, X. Chen, D. Nishio-Hamane, R. Arita, Y. Otani, S. Miwa, and S. Nakatsuji, "Perpendicular full switching of chiral antiferromagnetic order by current," Nature **607**, 474–479 (2022).

[3] R. Cheng, D. Xiao, and A. Brataas, "Terahertz antiferromagnetic spin hall nano-oscillator," Phys. Rev. Lett. **116**, 207603 (2016).

[4] K. Olejník, T. Seifert, Z. Kašpar, V. Novák, P. Wadley, R. P. Campion, M. Baumgartner, P. Gambardella, P. Němec, J. Wunderlich, J. Sinova, P. Kužel, M. Müller, T. Kampfrath, and T. Jungwirth, "Terahertz electrical writing speed in an antiferromagnetic memory," Science Advances **4**, eaar3566 (2018).

[5] R. Lebrun, A. Ross, S. A. Bender, A. Qaiumzadeh, L. Baldrati, J. Cramer, A. Brataas, R. A. Duine, and M. Kläui, "Tunable long-distance spin transport in a crystalline antiferromagnetic iron oxide," Nature **561**, 222–225 (2018).

[6] T. Jungwirth, X. Marti, P. Wadley, and J. Wunderlich, "Antiferromagnetic spintronics," Nature Nanotechnology **11**, 231–241 (2016).

[7] Y. J. Bae, J. Wang, A. Scheie, J. Xu, D. G. Chica, G. M. Diederich, J. Cenker, M. E. Ziebel, Y. Bai, H. Ren, C. R. Dean, M. Delor, X. Xu, X. Roy, A. D. Kent, and X. Zhu, "Exciton-coupled coherent magnons in a 2d semiconductor," Nature **609**, 282–286 (2022).

[8] W. Szuszkiewicz, B. Hennion, B. Witkowska, E. Łusakowska, and A. Mycielski, "Neutron scattering study of structural and magnetic properties of hexagonal MnTe," physica status solidi (c) **2**, 1141–1146 (2005).

[9] D. Kriegner, K. Výborný, K. Olejník, H. Reichlová, V. Novák, X. Marti, J. Gazquez, V. Saidl, P. Němec, V. V. Olobuev, G. Springholz, V. Holý, and T. Jungwirth, "Multiple-stable anisotropic

magnetoresistance memory in antiferromagnetic MnTe," Nature Communications **7**, 11623 (2016).

[10]J. Zhang, Q. Lian, Z. Pan, W. Bai, J. Yang, Y. Zhang, X. Tang, and J. Chu, "Spin-phonon coupling and two-magnons scattering behaviors in hexagonal NiAs-type antiferromagnetic MnTe epitaxial films," Journal of Raman Spectroscopy **51**, 1383–1389 (2020).

[11]D. Bossini, S. Dal Conte, M. Terschanski, G. Springholz, A. Bonanni, K. Deltenre, F. Anders, G. S. Uhrig, G. Cerullo, and M. Cinchetti, "Femtosecond phononic coupling to both spins and charges in a room-temperature antiferromagnetic semiconductor," Phys. Rev. B **104**, 224424 (2021).

[12]L. Šmejkal, J. Sinova, and T. Jungwirth, "Emerging research landscape of altermagnetism," Phys. Rev. X **12**, 040501 (2022).

[13]L. Šmejkal, J. Sinova, and T. Jungwirth, "Beyond conventional ferromagnetism and antiferromagnetism: A phase with nonrelativistic spin and crystal rotation symmetry," Phys. Rev. X **12**, 031042 (2022).

[14]J. Krampaský, L. Šmejkal, S. W. D'Souza, M. Hajlaoui, G. Springholz, K. Uhlířová, F. Alarab, P. C. Constantinou, V. Strocov, D. Usanov, W. R. Pudelko, R. González-Hernández, A. B. Hellenes, Z. Jansa, H. Reichlová, Z. Šobáň, R. D. G. Betancourt, P. Wadley, J. Sinova, D. Kriegner, J. Minár, J. H. Dil, and T. Jungwirth, "Altermagnetic lifting of Kramers spin degeneracy," Nature **626**, 517–522 (2024).

[15]Y. Zhu, X. Chen, X.-R. Liu, Y. Liu, P. Liu, H. Zha, G. Qu, C. Hong, J. Li, Z. Jiang, X.-M. Ma, Y.-J. Hao, M.-Y. Zhu, W. Liu, M. Zeng, S. Jayaram, M. Lenger, J. Ding, S. Mo, K. Tanaka, M. Arita, Z. Liu, M. Ye, D. Shen, J. Wrachtrup, Y. Huang, R.-H. He, S. Qiao, Q. Liu, and C. Liu, Nature **626**, 523–528 (2024).

[16]O. Fedchenko, J. Minár, A. Akashdeep, S. W. D'Souza, D. Vasilyev, O. Tkach, L. Odenbreit, Q. Nguyen, D. Kutnyakhov, N. Wind, L. Wenthaus, M. Scholz, K. Rossnagel, M. Hoesch, M. Aeschlimann, B. Stadtmüller, M. Kläui, G. Schönhense, T. Jungwirth, A. B. Hellenes, G. Jakob, L. Šmejkal, J. Sinova, and H.-J. Elmers, "Observation of time-reversal symmetry breaking in the band structure of altermagnetic RuO_2," Science Advances **10**, eadj4883 (2024), https://www.science.org/doi/pdf/10.1126/sciadv.adj4883.

[17]L. Šmejkal, A. Marmodoro, K.-H. Ahn, R. González-Hernández, I. Turek, S. Mankovsky, H. Ebert, S. W. D'Souza, O. c. v. Šipr, J. Sinova, and T. c. v. Jungwirth, "Chiral magnons in altermagnetic ruo_2," Phys. Rev. Lett. **131**, 256703 (2023).

[18]Z. Feng, X. Zhou, L. Šmejkal, L. Wu, Z. Zhu, H. Guo, R. González-Hernández, X. Wang, H. Yan, P. Qin, X. Zhang, H. Wu, H. Chen, Z. Meng, L. Liu, Z. Xia, J. Sinova, T. Jungwirth, and Z. Liu, "An anomalous hall effect in altermagnetic ruthenium oxide," Nature Electronics **5**, 735–743 (2022).

[19]Y. Liu, H. Bai, Y. Song, Z. Ji, S. Lou, Z. Zhang, C. Song, and Q. Jin, "Inverse altermagnetic spin splitting effect-induced terahertz emission in RuO2," Advanced Optical Materials **n/a**, 2300177 (2023), https://onlinelibrary.wiley.com/doi/pdf/10.1002/adom.202300177.

[20]H. Bai, L. Han, X. Y. Feng, Y. J. Zhou, R. X. Su, Q. Wang, L. Y. Liao, W. X. Zhu, X. Z. Chen, F. Pan, X. L. Fan, and C. Song, "Observation of spin splitting torque in a collinear antiferromagnet ruo_2," Phys. Rev. Lett. **128**, 197202 (2022).

[21]A. Bose, N. J. Schreiber, R. Jain, D.-F. Shao, H. P. Nair, J. Sun, D. A. Muller, E. Y. Tsymbal, D. G. Schlom, and D. C. Ralph, "Tilted spin current generated by the collinear antiferromagnet ruthenium dioxide," Nat. Electron. **5**, 267–274 (2022).

[22]R. D. Gonzalez Betancourt, J. Zubáč, R. Gonzalez-Hernandez, K. Geishendorf, Z. Šobáň, G. Springholz, K. Olejník, L. Šmejkal, J. Sinova, T. Jungwirth, S. T. B. Goennenwein, A. Thomas, H. Reichlová, J. Železný, and D. Kriegner, "Spontaneous anomalous Hall effect arising from an unconventional compensated magnetic phase in a semiconductor," Phys. Rev. Lett. **130**, 036702 (2023).

[23]I. I. Mazin, "Altermagnetism in MnTe: Origin, predicted manifestations, and routes to detwinning," Phys. Rev. B **107**, L100418 (2023).

[24]Y.-X. Yan, E. B. Gamble, and K. A. Nelson, "Impulsive stimulated scattering: general importance in femtosecond laser pulse interactions with matter, and spectroscopic applications," Journal of Chemical Physics **83**, 5391–5399 (1985).

[25]H. J. Zeiger, J. Vidal, T. K. Cheng, E. P. Ippen, G. Dresselhaus, and M. S. Dresselhaus, "Theory for displacive excitation of coherent phonons," Phys. Rev. B **45**, 768–778 (1992).

[26]D. Bossini, M. Terschanski, F. Mertens, G. Springholz, A. Abonanni, G. S. Uhrig, and M. Cinchetti, "Exchange-mediated magnetic blue-shift of the band-gap energy in the antferromagnetic semiconductor MnTe," New Journal of Physics **22**, 083029 (2020).

[27]K. Deltenre, D. Bossini, F. B. Anders, and G. S. Uhrig, "Lattice-driven femtosecond magnon dynamics in $\alpha-$MnTe," Phys. Rev. B **104**, 184419 (2021).

[28]C. Zhu, P. Pilch, A. Reinold, D. Kudlacik, G. Springholz, A. Bonanni, M. Assmann, M. Cinchetti, and Z. Wang, "Ultrafast dynamics of optically excited charge carriers in the room-

temperature antiferromagnetic semiconductor $\alpha-$MnTe," Phys. Rev. Mater. **7**, 054601 (2023).
[29]Note that GHz-scale *acoustic* phonons can be excited by laser light both above the bandgap, by the deformation potential mechanism (similar to DECP), and below the bandgap, by thermoelastic or electrostriction mechanisms (see *P. Ruello and V. E. Gusev, Ultrasonics 56, 21-35 (2015)* for a review.) Thus, the observation of similar-frequency acoustic phonons in both our work and Ref. 28 does not necessarily contradict the differing optical phonon measurements in our work and Ref. 11.
[30]E. G. Gamaly and A. V. Rode, "Physics of ultra-short laser interaction with matter: from phonon excitation to ultimate transformations," Progress in Quantum Electronics **37**, 215–323 (2013).
[31]S. Mu, R. P. Hermann, S. Gorsse, H. Zhao, M. E. Manley, R. S. Fishman, and L. Lindsay, "Phonons, magnons, and lattice thermal transport in antiferromagnetic semiconductor MnTe," Phys. Rev. Mater. **3**, 025403 (2019).
[32]D. Kriegner, H. Reichlova, J. Grenzer, W. Schmidt, E. Ressouche, J. Godinho, T. Wagner, S. Y. Martin, A. B. Shick, V. V. Volobuev, G. Springholz, V. Holý, J. Wunderlich, T. Jungwirth, and K. Výborný, "Magnetic anisotropy in antiferromagnetic hexagonal MnTe," Phys. Rev. B **96**, 214418 (2017).
[33]S. M. Rezende, A. Azevedo, and R. L. Rodríguez-Suárez, "Introduction to antiferromagnetic magnons," Journal of Applied Physics **126**, 151101 (2019).
[34]K. Yang, K. Kang, Z. Diao, A. Ramanathan, M. H. Karigerasi, D. P. Shoemaker, A. Schleife, and D. G. Cahill, "Magneto-optic response of the metallic antiferromagnet fe_2As to ultrafast temperature excursions," Phys. Rev. Mater. **3**, 124408 (2019).
[35]C. Tzschaschel, K. Otani, R. Iida, T. Shimura, H. Ueda, S. Günther, M. Fiebig, and T. Satoh, "Ultrafast optical excitation of coherent magnons in antiferromagnetic NiO," Phys. Rev. B **95**, 174407 (2017).
[36]I. Lyalin, S. Cheng, and R. K. Kawakami, "Spin-orbit torque in bilayers of kagome ferromagnet Fe_3Sn_2 and pt," Nano Letters **21**, 6975–6982 (2021).
[37]C. Berk, M. Jaris, W. Yang, S. Dhuey, S. Cabrini, and H. Schmidt, "Strongly coupled magnon-phonon dynamics in a single nanomagnet," Nature Communications **10**, 2652 (2019).
[38]D. M. Lattery, *Time-resolved magneto-optical Kerr effect for the study of ultrafast magnetization dynamics in magnetic thin films*, Phd thesis, University of Minnesota Twin Cities (2020).
[39]D.-L. Zhang, J. Zhu, T. Qu, D. M. Lattery, R. H. Victora, X. Wang, and J.-P. Wang, "High-frequency magnetoacoustic resonance through strain-spin coupling

in perpendicular magnetic multilayers," Science Advances **6**, eabb4607 (2020), https://www.science.org/doi/pdf/10.1126/sciadv.abb4607.

[40]S. A. McGill, R. I. Miller, O. N. Torrens, A. Mamchik, I.-W. Chen, and J. M. Kikkawa, "Dynamic Kerr effect and the spectral weight transfer of the manganites," Phys. Rev. Lett. **93**, 047402 (2004).

[41]M. Brahlek and M. Chilcote, private communication (2023).

[42]M. Djordjevic, M. Lüttich, P. Moschkau, P. Guderian, T. Kampfrath, R. G. Ulbrich, M. Münzenberg, W. Felsch, and J. S. Moodera, "Comprehensive view on ultrafast dynamics of ferromagnetic films," physica status solidi c **3**, 1347–1358 (2006).

[43]B. Mansart, M. J. G. Cottet, G. F. Mancini, T. Jarlborg, S. B. Dugdale, S. L. Johnson, S. O. Mariager, C. J. Milne, P. Beaud, S. Grübel, J. A. Johnson, T. Kubacka, G. Ingold, K. Prsa, H. M. Rønnow, K. Conder, E. Pomjakushina, M. Chergui, and F. Carbone, "Temperature-dependent electron-phonon coupling in $La_{2-x}Sr_xCuo_4$ probed by femtosecond x-ray diffraction," Phys. Rev. B **88**, 054507 (2013).

Supplemental Materials for "Time-resolved magneto-optical Kerr effect in the altermagnet candidate MnTe"

I. MAGNETIC FIELD DEPENDENCE OF OPTICAL PHONONS

In Fig. S1, we show short scans of $\Delta\theta_K(t)$ scans at H_{app} = +2.2 kG, 0 kG, and -2.2 kG out-of-plane, with corresponding FFTs. The oscillations repeat nearly point-for-point, showing no change with field. Therefore, we ascribe this signal purely to optical phonons and not phonon-induced magnons. Vertical dashed lines are drawn at f = 3.65 THz and f = 4.26 THz in S1(b) as a visual aid to show that the peaks do not shift.

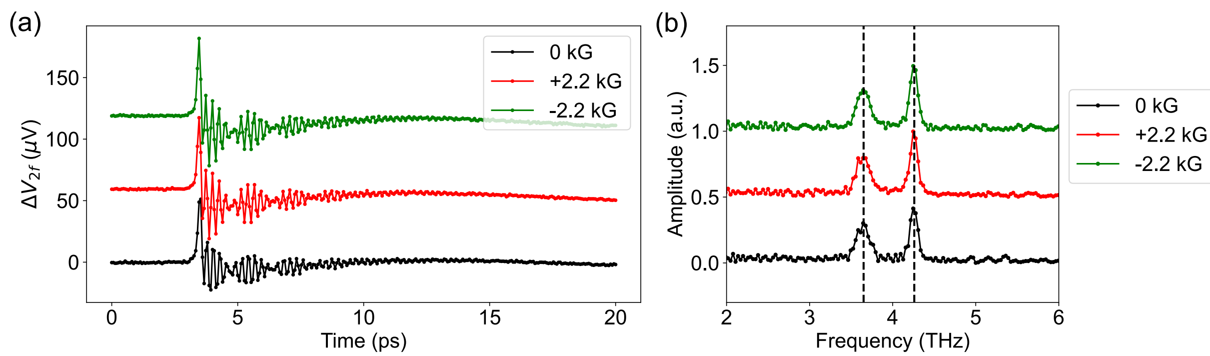

FIG. S1. (a) $\Delta\theta_K(t)$ time traces and (b) FFTs showing optical phonons at 295 K at H_{app} = +2.2 kG, 0 kG, and -2.2 kG out-of-plane.

II. LONG SCANS AT LOW TEMPERATURE

Here, we show long scans at low temperature at H_{app} = 500 G, demonstrating no spin oscillations. In Fig. S2(a), we show the full data set from Fig. 4 of the main text, which restricted the time extent to 20 ps so that the optical phonon oscillations could be more easily seen. In Fig. S2(b), we present a separate set of $\Delta\theta_K(t)$ scans with 133 ps time extent on the same sample, also with H_{app} = 500 G. Within experimental sensitivity ($\sim 1\mu$V), $\Delta\theta_K(t)$ is constant after electron-lattice relaxation.

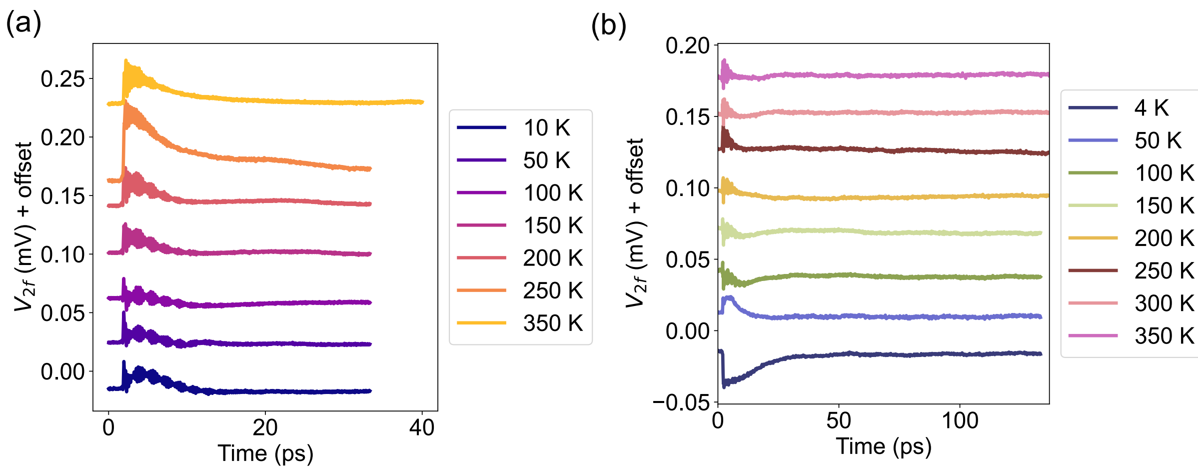

FIG. S2. (a) Full data set from Fig. 4(a) of the main text, with 35 ps time extent. (b) A separate temperature-dependent run with 133 ps time extent, showing no magnon oscillations.

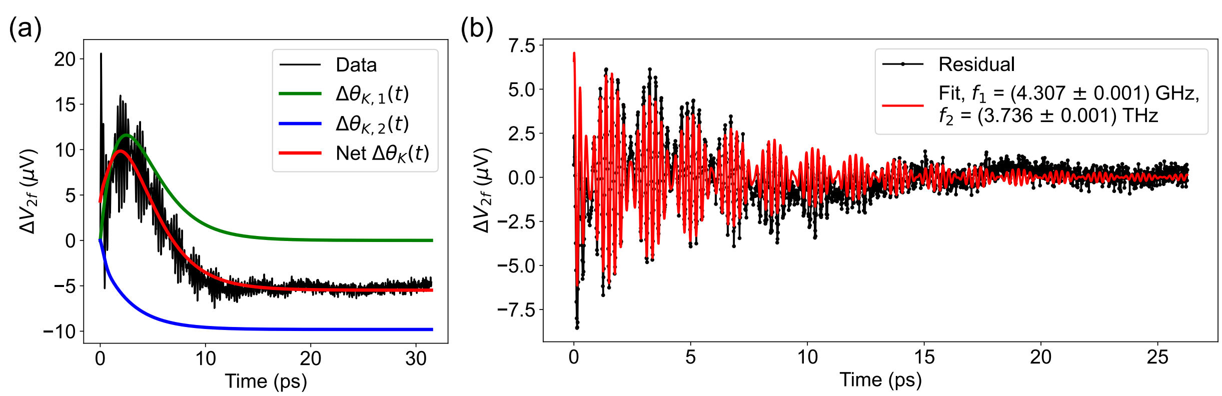

FIG. S3.

Fitting 10 K data from Fig. 4 of the main text. (a) Fitting the background to Eqn. 6. (b) Fitting the residual oscillations (with background subtracted) to two damped sinusoids.

III. FITTING TR-MOKE BACKGROUND AT LOW TEMPERATURES

In this section, we detail the fitting process for the low-temperature data in Fig. 4 of the main text. We show the fitting at 10 K; other temperatures are processed in exactly the same way. Fig. S3(a) shows the raw data at 10 K, the individual contributions from the best fit $\Delta\theta_{K,1}(t)$ and $\Delta\theta_{K,2}(t)$ from Eqn. 6, and their sum $\Delta\theta_{K,net}(t)$. In Fig. S3, we subtract the best-fit $\Delta\theta_{K_net}(t)$ background from the data and fit the residuals to $\Delta\theta_K(t) = A_1 e^{-\alpha_1 t}\sin(2\pi f_1 t + \phi_1) + A_2 e^{-\alpha_2 t}\sin(2\pi f_2 t + \phi_2)$.

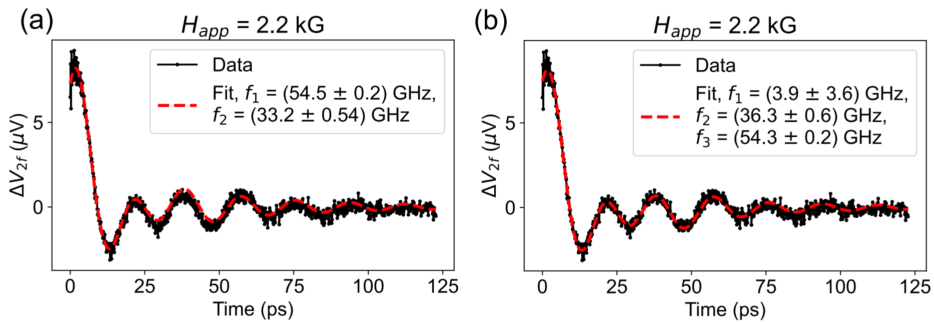

FIG. S4.

Fitting the data at H_{app} = +2.2 kG from Fig. 2(a) of the main text. At this pump angle (225°), three damped sines do not provide an improved fit compared to two damped sines.

IV. DETAILS OF FITTING MAGNETIC FIELD AND PUMP POLARIZATION DEPENDENCE

Here we provide details of the fitting of the spin oscillations as well as the optical phonon oscillations in Figs. 1 and 2 of the main text. In Fig. S4, we show an example of fitting the magnetic field dependence at fixed 225° pump angle in Fig. 2(a) of the main text. We fit to two damped sinusoids in Fig. S4(a) and three damped sinusoids in S4(b). In this set, a third oscillation is not well-resolved ($f_1 = 3.9 \pm 3.6$ GHz) and the quality of the fit is not improved. Data at other values of H_{app} in Fig. 2(a) shows similar behavior.

We then fit the pump polarization dependence in Fig. S5. We fit the spin oscillation at 75° pump angle to two and three sinusoids in S5(a) and (b), respectively, and compare to similar fits of the oscillation at 195° pump angle in (c) and (d). In the 75° data, three frequencies, fitting to 25, 43, and 55 GHz, are better than two, while in the 195° data, the fits are nearly identical and $f_3 = 58 \pm 5$ GHz is not well-distinguished from $f_1 = 51.8 \pm 0.2$ GHz. This suggests that there are at least three frequencies - likely one magnon and two acoustic phonons - with different pump angle dependence. Finally, we fit the optical phonon pump dependence from Fig. 1(c) of the main text to two damped sinusoids, showing an example at 195° in Fig. S5(e). We plot the resulting fit amplitudes A_1 and A_2 as a function of pump angle in S5(f), and in turn fit those amplitudes to $\sin(3\theta)$ to test for three-fold symmetry. While A_1 is inconclusive, A_2 indeed exhibits three-fold symmetry.

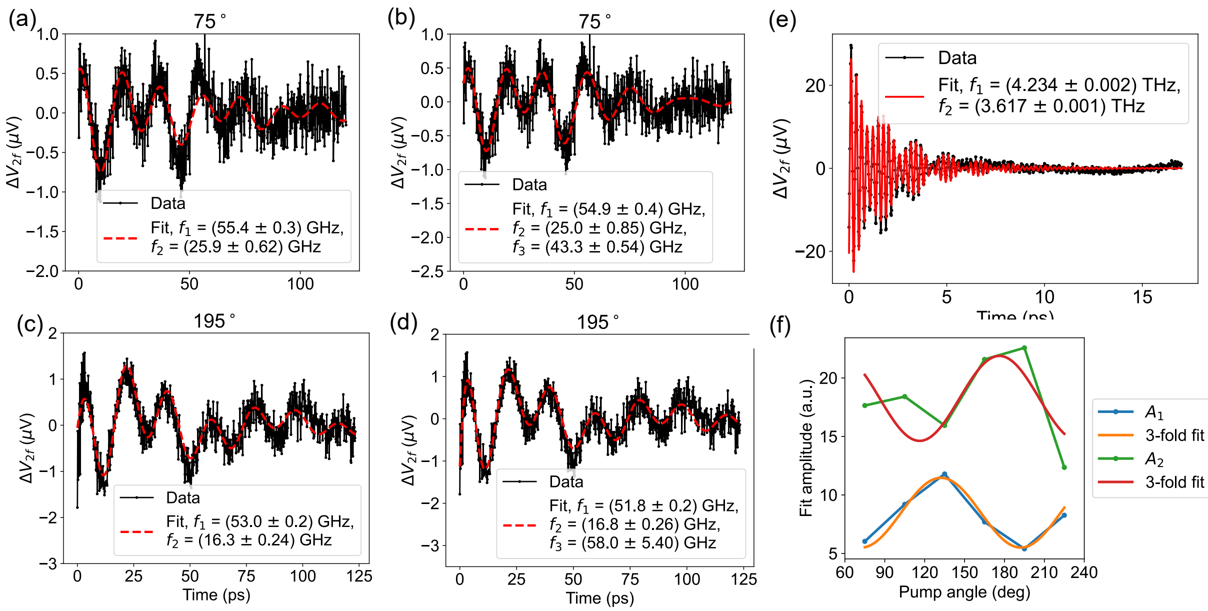

FIG. S5.

Fitting polarization dependence from Fig. 1 and 2 of the main text. (a,b) Fitting the spin oscillation data at 75° pump angle to two and three damped sinusoids, respectively. (c,d) Repeating the process at 195° pump angle. While three sinusoids fit better than two at 75°, no noticable improvement is seen at 195°. (e) Example fit of the optical phonon data at 195° pump angle to two damped sinusoids. (f) Resulting fit amplitudes as a function of angle, together with fits to three-fold symmetry ($\sin 3\theta$).